Eur. Phys. J. Appl. Phys. **31**, 3–9 (2005)
DOI: 10.1051/epjap:2005035

THE EUROPEAN PHYSICAL JOURNAL
APPLIED PHYSICS

Polarimetric scattering from a layer of spatially oriented metamaterial small spheroids

H.-X. Ye and Y.-Q. Jin[a]

Key Laboratory of Wave Scattering and Remote Sensing Information (Ministry of Education), Fudan University, Shanghai 200433, P.R. China

Received: 18 August 2004 / Received in final form: 24 December 2004 / Accepted: 11 February 2005
Published online: 27 April 2005 –

Abstract. Complex scattering amplitude functions of a small metamaterial spheroid are derived. The Mueller matrix solution for polarimetric bistatic scattering from a layer of random metamaterial small spheroids is then constructed. Bistatic scattering of metamaterial and dielectric spheroids are numerically calculated. Linearly co-polarized backscattering coefficients σ_{hh}, σ_{vv} and $\sigma_{hh} - \sigma_{vv}$ are presented to show the dependence upon frequency. The co-polarized and cross-polarized backscattering coefficients and polarizability degree of a layer of non-uniformly oriented metamaterial spheroids under illumination of an elliptic polarized plane wave are numerically simulated. Effects of metamaterial parameters on scattering pattern and scattering mechanism are interpreted. Numerical results indicate that the bistatic scattering of metamaterial particles is enhanced largely and demonstrates asymmetric directivity. Meanwhile, polarized difference of $\sigma_{hh} - \sigma_{vv}$ strongly varies with frequency due to constitutive dispersion of $\varepsilon(\omega)$ and $\mu(\omega)$.

PACS. 42.25.Dd Wave propagation in random media – 42.68.Ay Propagation, transmission, attenuation, and radiative transfer – 42.68.Mj Scattering, polarization – 33.15.Kr Electric and magnetic moments (and derivatives), polarizability, and magnetic susceptibility

1 Introduction

In early 1968, Vesalago [1] proposed a medium with both the permittivity ε and permeability μ as negative, and studied electromagnetic (EM) wave propagation with abnormal phenomena, e.g. opposite directivity of the phase velocity and Poynting vector, reversal of Doppler shift, and anomalous refraction at the boundary of the media. These phenomena have been remained for verification, even though the ionosphere has been found with negative $\varepsilon_{eff}(\omega)$ in case of low frequency below the plasma frequency [2]. In late 1996 [3] and 1999 [4], Pendry et al. suggested that an array of metal wires and split ring resonators (SRRs), respectively, exhibit negative effective permittivity $\varepsilon < 0$ and permeability $\mu < 0$ when frequency is close to the resonance frequency of these cells. In 2001, Smith [5] et al. constructed a metamaterial of $\varepsilon < 0$ and $\mu < 0$ with a periodical array of SRRs and thin wires, and experimentally demonstrated the negative refraction phenomena. From then on, metamaterial has attracted great attention in many fields, such as electromagnetics, materials science, electronics, and potential applications are also studied, for example, such as high directivity antenna, perfect lens [6], phase compensator [7], etc.

This kind of material was named by Vesalago as Left-Handed Media (LHM), because the vectors $\bar{E}$, $\bar{H}$ and $\hat{k}$ form a left-handed triplet instead of a right-handed triplet [1] as in the conventional Right-Handed Media (RHM). Sometimes, this material is also called as Negative Refractive Index Material, Backward Wave Medium, Double Negative Material and some others.

However most researches are limited to study of the effective permittivity and propagation through an infinite metamaterial medium [6,7]. No discussion has been studied for polarimetric scattering from a layer of metamaterial particulate media. In polarimetric scattering and radiative transfer from a layer of random medium, the 2×2-dimensional (-D) complex scattering amplitude functions and the 4×4-D Mueller matrix for Stokes scattered vector can be measured by the polarimetry technique such as synthetic aperture radar (SAR) imagery technology [8]. Jin presented a Mueller matrix solution for numerical simulation of polarimetric scattering from a layer of random and non-uniformly oriented non-spherical particles [8,9,11]. Co-polarized and cross-polarized bistatic scattering coefficients can be numerically calculated.

This paper derives the complex scattering amplitude functions of random metamaterial small spheroids under the Rayleigh approximation, and then constructs the Mueller matrix. The bistatic scattering from a layer of

[a] e-mail: yqjin@fudan.ac.cn

random metamaterial small spheroids over an underlying medium are numerically simulated. Variations of horizontally ($\hat{h}$) and vertically ($\hat{v}$) co-polarized backscattering coefficients σ_{hh}, σ_{vv} and their difference $\sigma_{hh} - \sigma_{vv}$ upon frequency are obtained. Scattering patterns of co-polarized backscattering σ_c, cross-polarized σ_x and polarizability degree m_s of a layer of random metamaterial small spheroids under illumination of an elliptically polarized wave are demonstrated.

2 Polarizability matrix of bianisotropic spheroids

The macroscopic constitutive relations of bianisotropic media are generally written as

$$\begin{cases} \bar{D} = \bar{\bar{\varepsilon}} \cdot \bar{E} + \bar{\bar{\xi}} \cdot \bar{H} = \varepsilon_0 \bar{E} + \bar{P}_e \\ \bar{B} = \bar{\bar{\varsigma}} \cdot \bar{E} + \bar{\bar{\mu}} \cdot \bar{H} = \mu_0 \bar{H} + \bar{P}_m \end{cases} \tag{1}$$

where $\bar{\bar{\varepsilon}}$, $\bar{\bar{\xi}}$, $\bar{\bar{\varsigma}}$ and $\bar{\bar{\mu}}$ are 3×3-D matrices, $\bar{E}$ and $\bar{H}$ are the electric and magnetic fields, $\bar{D}$ and $\bar{B}$ are the electric and magnetic displacements, $\bar{P}_e$ and $\bar{P}_m$ are polarization and magnetization dyadics, respectively. Equation (1) can yield

$$\begin{cases} \bar{P}_e = \left(\bar{\bar{\varepsilon}} - \varepsilon_0 \bar{\bar{I}}\right) \cdot \bar{E} + \bar{\bar{\xi}} \cdot \bar{H} \\ \bar{P}_m = \bar{\bar{\varsigma}} \cdot \bar{E} + \left(\bar{\bar{\mu}} - \mu_0 \bar{\bar{I}}\right) \cdot \bar{H} \end{cases} \tag{2}$$

where $\bar{\bar{I}}$ is unit diagonal matrix.

Under the Rayleigh approximation for small particle, the internal fields inside a small spheroid (its semi-axes are, respectively, a, b and c) can be obtained as [12]

$$\begin{cases} \bar{E} = \bar{E}_i - \frac{\bar{\bar{L}}}{\varepsilon_0} \cdot \bar{P}_e \\ \bar{H} = \bar{H}_i - \frac{\bar{\bar{L}}}{\mu_0} \cdot \bar{P}_m \end{cases} \tag{3}$$

where $\bar{E}_i$ and $\bar{H}_i$ are incident fields, the depolarization dyadic $\bar{\bar{L}}$ is written as

$$\bar{\bar{L}} = g_1 \hat{x}_b \hat{x}_b + g_2 \hat{y}_b \hat{y}_b + g_3 \hat{z}_b \hat{z}_b \tag{4}$$

here $g_i (i = 1, 2, 3)$ is related to the geometrical dimension of the spheroid, and its expression can be found in reference [9]. The local coordinates $(\hat{x}_b, \hat{y}_b, \hat{z}_b)$ defined by the semi-axes of the spheroid can be transformed into the principal coordinates $(\hat{x}, \hat{y}, \hat{z})$ by rotations of the Euler angles (α, β, γ).

From equations (2, 3), it is derived to obtain

$$\left[\bar{\bar{I}} + \left(\bar{\bar{\varepsilon}}_r - \bar{\bar{I}}\right) \cdot \bar{\bar{L}} - \bar{\bar{\xi}}_r \cdot \bar{\bar{L}} \cdot \left(\bar{\bar{I}} + \bar{\bar{\mu}}_r \cdot \bar{\bar{L}} - \bar{\bar{L}}\right)^{-1} \cdot \bar{\bar{\varsigma}}_r \cdot \bar{\bar{L}}\right] \cdot \bar{P}_e =$$

$$\varepsilon_0 \left[\bar{\bar{\varepsilon}}_r - \bar{\bar{I}} - \bar{\bar{\xi}} \cdot \bar{\bar{L}} \cdot \left(\bar{\bar{I}} + \bar{\bar{\mu}}_r \cdot \bar{\bar{L}} - \bar{\bar{L}}\right)^{-1} \cdot \bar{\bar{\varsigma}}_r \cdot \bar{\bar{L}}\right] \cdot \bar{E}_i$$

$$+ \sqrt{\varepsilon_0 \mu_0} \bar{\bar{\xi}}_r \cdot \left[\bar{\bar{I}} - \bar{\bar{L}} \cdot \left(\bar{\bar{I}} + \bar{\bar{\mu}}_r \cdot \bar{\bar{L}} - \bar{\bar{L}}\right)^{-1} \cdot \left(\bar{\bar{\mu}}_r - \bar{\bar{I}}\right)\right] \cdot \bar{H}_i \tag{5}$$

$$\left[\bar{\bar{I}} + \left(\bar{\bar{\mu}}_r - \bar{\bar{I}}\right) \cdot \bar{\bar{L}} - \bar{\bar{\varsigma}}_r \cdot \bar{\bar{L}} \cdot \left(\bar{\bar{I}} + \bar{\bar{\varepsilon}}_r \cdot \bar{\bar{L}} - \bar{\bar{L}}\right)^{-1} \cdot \bar{\bar{\xi}}_r \cdot \bar{\bar{L}}\right] \cdot \bar{P}_m =$$

$$\mu_0 \left[\bar{\bar{\mu}}_r - \bar{\bar{I}} - \bar{\bar{\varsigma}}_r \cdot \bar{\bar{L}} \cdot \left(\bar{\bar{I}} + \bar{\bar{\varepsilon}}_r \cdot \bar{\bar{L}} - \bar{\bar{L}}\right)^{-1} \cdot \bar{\bar{\xi}}_r \cdot \bar{\bar{L}}\right] \cdot \bar{H}_i$$

$$+ \sqrt{\varepsilon_0 \mu_0} \bar{\bar{\varsigma}}_r \cdot \left[\bar{\bar{I}} - \bar{\bar{L}} \cdot \left(\bar{\bar{I}} + \bar{\bar{\varepsilon}}_r \cdot \bar{\bar{L}} - \bar{\bar{L}}\right)^{-1} \cdot \left(\bar{\bar{\varepsilon}}_r - \bar{\bar{I}}\right)\right] \cdot \bar{E}_i \tag{6}$$

where $\bar{\bar{\varepsilon}}_r = \bar{\bar{\varepsilon}}/\varepsilon_0$, $\bar{\bar{\mu}}_r = \bar{\bar{\mu}}/\mu_0$, $\bar{\bar{\xi}}_r = \bar{\bar{\xi}}/\sqrt{\varepsilon_0 \mu_0}$, $\bar{\bar{\varsigma}}_r = \bar{\bar{\varsigma}}/\sqrt{\varepsilon_0 \mu_0}$.

Supposing the uniform distribution of $\bar{P}_e$ and $\bar{P}_m$ inside the spheroid, the electric and magnetic dipole moments $\bar{p}$ and $\bar{m}$ are expressed as follows

$$\begin{cases} \bar{p} = V \bar{P}_e = \bar{\bar{\alpha}}_{ee} \cdot \bar{E}_i + \bar{\bar{\alpha}}_{em} \cdot \bar{H}_i \\ \bar{m} = V \bar{P}_m = \bar{\bar{\alpha}}_{me} \cdot \bar{E}_i + \bar{\bar{\alpha}}_{mm} \cdot \bar{H}_i \end{cases} \tag{7}$$

where $\bar{\bar{\alpha}}_{ee}$, $\bar{\bar{\alpha}}_{em}$, $\bar{\bar{\alpha}}_{me}$, $\bar{\bar{\alpha}}_{mm}$ are the polarizability matrices, $V = (4\pi/3)abc$ is the volume of a spheroid. Because of the reciprocity of artificial synthetic metamaterial $\bar{\bar{\varepsilon}}_r = \bar{\bar{\varepsilon}}_r^t$, $\bar{\bar{\mu}}_r = \bar{\bar{\mu}}_r^t$, $\bar{\bar{\xi}}_r = -\bar{\bar{\varsigma}}_r^t$ [12,13] and shape symmetry of the spheroid, the polarizability matrices also satisfy the symmetric relations such as $\bar{\bar{\alpha}}_{ee} = \bar{\bar{\alpha}}_{ee}^t$, $\bar{\bar{\alpha}}_{mm} = \bar{\bar{\alpha}}_{mm}^t$ and $\bar{\bar{\alpha}}_{em} = -\bar{\bar{\alpha}}_{me}^t$, where the superscript t denotes the transpose.

The problem of chirality generated from the coupling factors $\bar{\bar{\xi}}_r$ and $\bar{\bar{\varsigma}}_r$ had been discussed in reference [8]. In this paper, $\bar{\bar{\varepsilon}}_r$ and $\bar{\bar{\mu}}_r$ are assumed as diagonal and the coupling $\bar{\bar{\xi}}_r$ and $\bar{\bar{\varsigma}}_r$ are simply neglected. Thus, the polarizability matrices are reduced to diagonal and the diagonal elements are written as

$$\alpha_{een} = \varepsilon_0 \frac{\varepsilon_{rn} - 1}{1 + (\varepsilon_{rn} - 1) g_n} \frac{4\pi}{3} abc \tag{8}$$

$$\alpha_{mmn} = \mu_0 \frac{\mu_{rn} - 1}{1 + (\mu_{rn} - 1) g_n} \frac{4\pi}{3} abc \tag{9}$$

$$\alpha_{emn} = \alpha_{men} = 0 \tag{10}$$

where $n = 1, 2, 3$.

3 The Mueller matrix for a layer of spatially oriented metamaterial spheroids

The scattering field from a scatter particle under $\bar{E}_{inc}$ incidence is written as

$$\bar{E}_s(\bar{r}) = \begin{bmatrix} E_{vs} \\ E_{hs} \end{bmatrix} = \frac{e^{ik_0 r}}{r} \begin{bmatrix} f_{vv} & f_{vh} \\ f_{hv} & f_{hh} \end{bmatrix} \begin{bmatrix} E_{vi} \\ E_{hi} \end{bmatrix}$$

$$= \frac{e^{ik_0 r}}{r} \bar{\bar{f}} \cdot \bar{E}_{inc} \tag{11}$$

where $\overline{\overline{f}}$ is the complex scattering amplitude function matrix, the subscripts v and h denote the vertical and horizontal polarizations respectively. Under the Rayleigh approximation, the scattering field can be expressed by the scattering from the electric and magnetic dipoles [12] as follows.

$$\bar{E}_s(\bar{r}) = \frac{e^{ik_0 r}}{4\pi r}\left[\omega^2\mu_0\left(\overline{\overline{I}} - \hat{k}_s\hat{k}_s\right)\cdot\bar{p} - \omega k_0\hat{k}_s\times\bar{m}\right] \quad (12)$$

where $\hat{k}_s$ is unit vector in scattering direction, ω is angular frequency.

The scattering amplitude functions of a scatter spheroid, such as oblate ($a = b \gg c$) or prolate ($a = b \ll c$) spheroid, are derived from equations (7, 12)

$$f_{vv} = \frac{3}{2k_0}\Big\{\left[t_{e1}\left(\hat{v}_s\cdot\hat{v}_i\right) + \left(t_{e0}-t_{e1}\right)\left(\hat{v}_s\cdot\hat{z}_b\right)\left(\hat{z}_b\cdot\hat{v}_i\right)\right] + \left[t_{m1}\left(\hat{h}_s\cdot\hat{h}_i\right) + \left(t_{m0}-t_{m1}\right)\left(\hat{h}_s\cdot\hat{z}_b\right)\left(\hat{z}_b\cdot\hat{h}_i\right)\right]\Big\} \quad (13)$$

$$f_{vh} = \frac{3}{2k_0}\Big\{\left[t_{e1}\left(\hat{v}_s\cdot\hat{h}_i\right) + \left(t_{e0}-t_{e1}\right)\left(\hat{v}_s\cdot\hat{z}_b\right)\left(\hat{z}_b\cdot\hat{h}_i\right)\right] - \left[t_{m1}\left(\hat{h}_s\cdot\hat{v}_i\right) + \left(t_{m0}-t_{m1}\right)\left(\hat{h}_s\cdot\hat{z}_b\right)\left(\hat{z}_b\cdot\hat{v}_i\right)\right]\Big\} \quad (14)$$

$$f_{hv} = \frac{3}{2k_0}\Big\{\left[t_{e1}\left(\hat{h}_s\cdot\hat{v}_i\right) + \left(t_{e0}-t_{e1}\right)\left(\hat{h}_s\cdot\hat{z}_b\right)\left(\hat{z}_b\cdot\hat{v}_i\right)\right] - \left[t_{m1}\left(\hat{v}_s\cdot\hat{h}_i\right) + \left(t_{m0}-t_{m1}\right)\left(\hat{v}_s\cdot\hat{z}_b\right)\left(\hat{z}_b\cdot\hat{h}_i\right)\right]\Big\} \quad (15)$$

$$f_{hh} = \frac{3}{2k_0}\Big\{\left[t_{e1}\left(\hat{h}_s\cdot\hat{h}_i\right) + \left(t_{e0}-t_{e1}\right)\left(\hat{h}_s\cdot\hat{z}_b\right)\left(\hat{z}_b\cdot\hat{h}_i\right)\right] + \left[t_{m1}\left(\hat{v}_s\cdot\hat{v}_i\right) + \left(t_{m0}-t_{m1}\right)\left(\hat{v}_s\cdot\hat{z}_b\right)\left(\hat{z}_b\cdot\hat{v}_i\right)\right]\Big\} \quad (16)$$

$$t_{e0} = \frac{2k_0^3a^2c}{9}\frac{\varepsilon_{r3}-1}{1+\left(\varepsilon_{r3}-1\right)g_3},$$
$$t_{e1} = \frac{2k_0^3a^2c}{9}\frac{\varepsilon_{r1}-1}{1+\left(\varepsilon_{r1}-1\right)g_1} \quad (17)$$

$$t_{m0} = \frac{2k_0^3a^2c}{9}\frac{\mu_{r3}-1}{1+\left(\mu_{r3}-1\right)g_3},$$
$$t_{m1} = \frac{2k_0^3a^2c}{9}\frac{\mu_{r1}-1}{1+\left(\mu_{r1}-1\right)g_1}. \quad (18)$$

Here the horizontal and vertical polarization vectors are defined as

$$\hat{h}_d = \frac{\hat{z}\times\hat{k}_d}{|\hat{z}\times\hat{k}_d|}, \quad \hat{v}_d = \hat{h}_d\times\hat{k}_d \quad (d\equiv s,i). \quad (19)$$

In order to apply the optical theorem for accurate calculation of the extinction coefficient, a high-order imaginary term should be supplemented into equations (13–16) of the Rayleigh approximation [12], i.e. t is rewritten as

$$T = t(1+it) \quad (20)$$

where t represents t_{e0}, t_{e1}, t_{m0} and t_{m1} [9,10].

In expressions (13–16), the scattering amplitude functions are related to Euler angles $\beta \in (\beta_1,\beta_2)$ and $\gamma \in (\gamma_1,\gamma_2)$ (note that for spheroid α will not appear), and the ensemble average over non-uniform orientation distribution of Euler angles is written as [9]

$$\langle f(\beta,\gamma)\rangle = \frac{1}{\cos\beta_1-\cos\beta_2} \times \int_{\beta_1}^{\beta_2} p(\beta)\sin\beta d\beta \frac{1}{\gamma_2-\gamma_1}\int_{\gamma_1}^{\gamma_2} p(\gamma)f(\beta,\gamma)d\gamma \quad (21)$$

where $p(\beta)$ and $p(\gamma)$ are the probability density functions of orientation.

The first-order Mueller matrix solution from vector radiative transfer for polarimetric scattering has been given by references [9,11]:

$$\overline{I}_s = \overline{\overline{M}}(\theta_s,\varphi_s;\theta_i,\varphi_i)\cdot\overline{I_i} \quad (22)$$

where $\overline{I}_s = [I_{vs}, I_{hs}, U_s, V_s]^T$ and $\overline{I}_i = [I_{vi}, I_{hi}, U_i, V_i]^T$ are, respectively, the scattering and incident stokes vectors. The Mueller matrix $\bar{\bar{M}}$, which describes particles single-scattering and the interactions with the interfaces, contains the eigen-matrix $\bar{\bar{E}}$, the phase matrix $\bar{\bar{P}}$ of the particles, diagonal propagation matrix $\bar{\bar{D}}$ and the reflectivity matrix $\bar{\bar{R}}$ of the underlying surface. $\bar{\bar{E}}$ and $\bar{\bar{D}}$ can be constructed by $\langle\overline{\overline{f}}(\theta_i,\varphi_i;\theta_i,\varphi_i)\rangle$ in forward direction, $\bar{\bar{P}}(\theta_s,\varphi_s;\theta_i,\varphi_i)$ is expressed by $\langle f_{pq}(\theta_s,\varphi_s;\theta_i,\varphi_i)f^*_{st}(\theta_s,\varphi_s;\theta_i,\varphi_i)\rangle(p,q,s,t = v,h)$ [11]. The co-polarized and cross-polarized scattering coefficients can be calculated from the Mueller matrix solution equation (22).

$$\sigma_c = 4\pi\cos\theta_s P_n \quad (23)$$

$$\sigma_x = 4\pi\cos\theta_s\left[I_{vs} + I_{hs} - P_n\right] \quad (24)$$

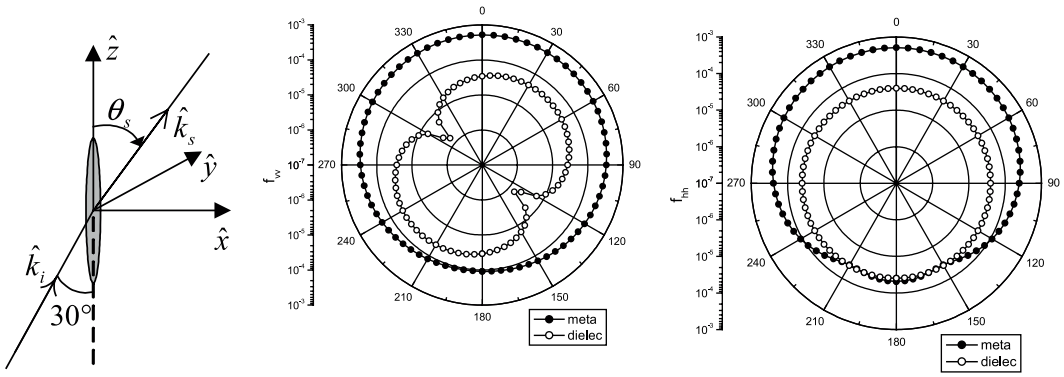

Fig. 1. Scattering amplitude functions of metamaterial and dielectric spheroids.

where

$$P_n = I_{vs}I_{vi} + I_{hs}I_{hi} - \frac{1}{2}U_sU_i + \frac{1}{2}V_sV_i \tag{25}$$

$$\begin{bmatrix} I_{vi} \\ I_{hi} \\ U_i \\ V_i \end{bmatrix} = \frac{1}{2}\begin{bmatrix} 1-\cos 2\chi\cos 2\psi \\ 1+\cos 2\chi\cos 2\psi \\ -2\cos 2\chi\sin 2\psi \\ 2\sin 2\chi \end{bmatrix}. \tag{26}$$

Here χ and ψ are, respectively, the elliptic and orientation angles of incident elliptical polarization [9].

4 Numerical results

The scattering amplitude functions of both the metamaterial and dielectric prolate spheroids ($a = 0.1$ cm, $c = 1.5$ cm) are calculated at $\theta_i = 30°$, $f = 7$ GHz. The constructive parameters are taken as

$$\begin{cases} \varepsilon_{xx} = \varepsilon_{yy} = -1.4 - j4.8 \\ \mu_{xx} = \mu_{yy} = -1.8 - j2.5 \end{cases} \quad (metamaterial)$$

$$\begin{cases} \varepsilon_{xx} = \varepsilon_{yy} = 1.45 \\ \mu_{xx} = \mu_{yy} = 1.0 \end{cases} \quad (dielectric).$$

Figure 1 compares the scattering amplitude functions $|f_{vv}|$ and $|f_{hh}|$ on the incident plane (i.e. $\varphi_s - \varphi_i = 0, \pi$) for metamaterial (solid circle line) and dielectric (no-filled circle line) spheroids. At this case, f_{vh} and f_{hv} are almost zero. It can be seen that scattering patterns of both $|f_{vv}|$ and $|f_{hh}|$ of the dielectric spheroid are symmetric along the incident direction. And $|f_{vv}|$ is strong in forward and backward direction (i.e. $\theta_s = 30°, \theta_s = 210°$, respectively), $|f_{hh}|$ is almost uniform in all directions. But, as a comparison, scattering patterns of both $|f_{vv}|$ and $|f_{hh}|$ of the metamaterial spheroid are symmetric along the spheroid axis $\hat{z}$. And $|f_{vv}|$ and $|f_{hh}|$ are strong around $\theta_s = 0°$ and become weaker around $\theta_s = 180°$ (one order less than $\theta_s = 0°$).

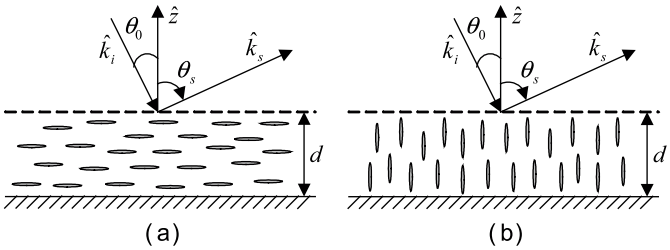

Fig. 2. Geometric model of a layer of random and horizontally or vertically aligned spheroids.

Conventional dielectric spheroid excited by incident EM wave generates polarization and its polarization direction is along the incident electric field $\overline{E}_i$. But the metamaterial spheroid excited by the incidence generates both polarization and magnetization, which are, respectively, opposite to the direction of the incident $\overline{E}_i$ and $\overline{H}_i$ due to negative ε' and μ'. It is a reason why the electric and magnetic dipole moments inside the spheroid are strong around $\theta_s = 0°$ and weak around $\theta_s = 180°$.

Bistatic scattering from a layer of horizontally ($\beta = 90°$) and vertically ($\beta = 0°$) aligned prolate spheroids over an underlying perfectly conducting surface is calculated. The models are shown in Figure 2. The following parameters are taken: uniform $\gamma \in (0°, 360°)$, particle fractional volume $f_s = 0.1$, layer thickness $d = 30$ cm, frequency of incident wave $f = 7$ GHz, and incident angle $\theta_0 = 30°(\theta_i = \pi - \theta_0)$. The bistatic scattering coefficients $\sigma_c(\theta_s, \theta_0 = 30°)$ of metamaterial and dielectric spheroids on the incident plane are presented in Figure 3.

It can be seen that co-polarized scattering of metamaterial spheroids (solid circle line) are apparently stronger than dielectric spheroids (no-filled circle line). Especially, in the case of horizontal orientation ($\beta = 90°$) scattering from metamaterial spheroids is much stronger at $\theta_s > 0$ than at $\theta_s < 0$ (in Figs. 3a, c).

It might be interpreted by Figure 4a that as an EM wave is incident upon, two main rays of scattering wave come from forward direction due to scattering of the particle and multi-reflections of particle-underlying surface

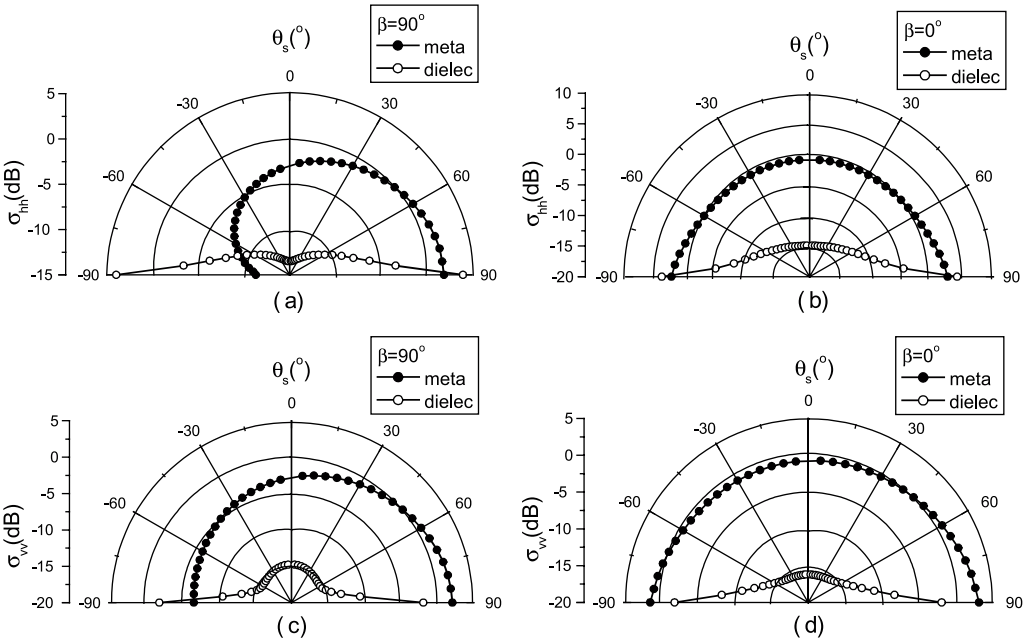

Fig. 3. σ_{vv} and σ_{hh} vs. scattering angles θ_s.

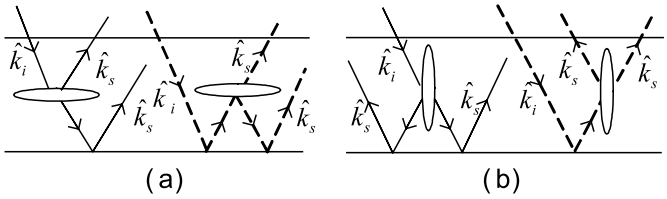

Fig. 4. Main rays of scattering from spheroids.

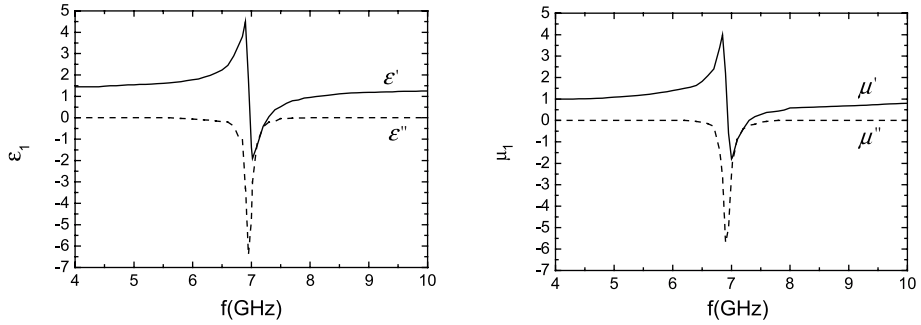

Fig. 5. Constructive parameters ε_1 and μ_1 of metamaterial.

(see the solid line and dashed line in Fig. 4a). All of them contribute to the forward direction ($\theta_s > 0$).

In another case of vertical orientation indicated by$\beta = 0°$, main rays as shown in Figure 4b contribute to forward and backward directions in couple, and yield equal scattering at θ_s and $-\theta_s$ as shown in Figures 3b and d.

Due to dispersion of artificially synthesized metamaterial, the permittivity ε and permeability μ become simultaneously negative at specific frequencies. Suppose to have $\varepsilon_{xx} = \varepsilon_{yy} = \varepsilon_1$, $\mu_{xx} = \mu_{yy} = \mu_1$ of metamaterial as cited in reference [14] shown in Figure 5, and $\varepsilon_{zz} = 1.5$, $\mu_{zz} = 1.0$, which are simply invariant with frequency. As a contrast, the spheroid scatters with isotropic permittivity of Lorentzian dielectric FR-4 [15] and dispersive relation of

$$\varepsilon_r(\omega) = \varepsilon_\infty + \frac{(\varepsilon_s - \varepsilon_\infty) f_p^2}{f_0^2 - f^2 + j \cdot f \cdot \Delta f} \tag{27}$$

are also compared. Here $\varepsilon_\infty = 4.181$, $\varepsilon_s = 4.307$, $f_0 = f_p = 17$ GHz, $\Delta f = 150$ GHz, and $\mu_r = 1$.

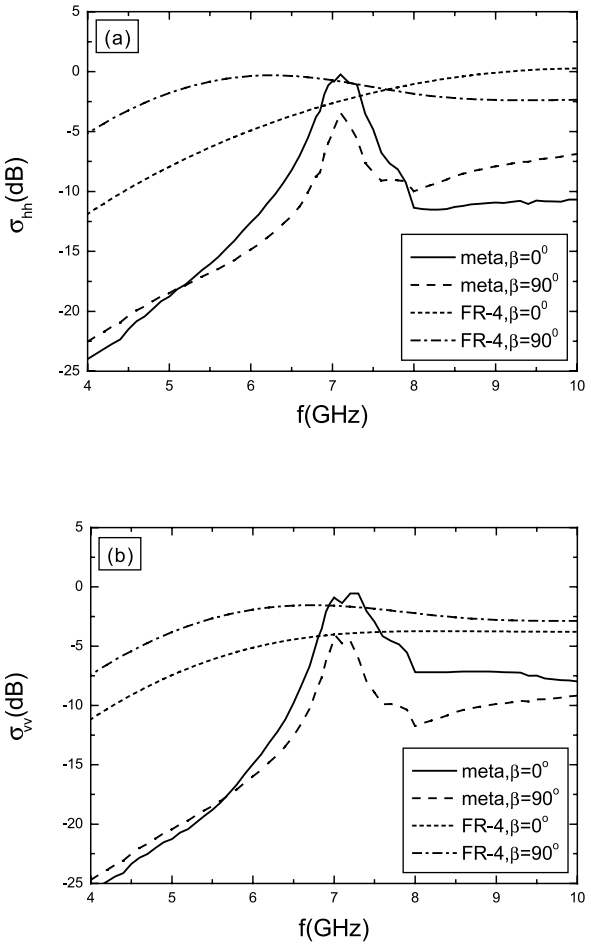

Fig. 6. Variation of backscattering coefficients σ_{hh} (a) and σ_{vv} (b) vs. frequency.

Figure 6 shows variation of co-polarized backscattering coefficients σ_{hh} and σ_{vv} of a layer of random, horizontally ($\beta = 90°$) and vertically ($\beta = 0°$) aligned metamaterial (solid points) and dielectric (hollow points) spheroids vs. frequency. At the frequencies to make ε_r and μ_r as negative, σ_{hh} and σ_{vv} of metamaterial spheroids increase quickly, especially for the case of $\beta = 0°$, and take peaks around $f = 7$ GHz because of the dispersion of ε and μ indicated in Figure 5. But the σ_{hh} and σ_{vv} of dielectric FR-4 change slightly with frequency.

Figure 7 compares the difference $\sigma_{hh} - \sigma_{vv}$ of metamaterial and dielectric FR-4 spheroids layer with $\beta = 0°$ and $\beta = 90°$ orientation distributions. The results indicate that the $\sigma_{hh} - \sigma_{vv}$ of metamaterial spheroids varies remarkably with frequency, and takes a peak around $f =$ 7.1 GHz, which happens to be the resonance frequency of metamaterial as shown in Figure 5. But $\sigma_{hh} - \sigma_{vv}$ of dielectric spheroids varies slightly with frequency, although it is dispersive.

Figures 8 and 9 show backscattering σ_c, σ_x and m_s vs. polarization angles (χ, ψ) when the metamaterial

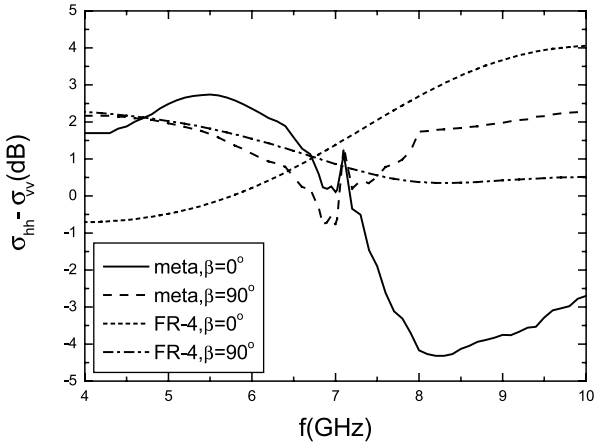

Fig. 7. Variation of $\sigma_{hh} - \sigma_{vv}$ of a layer of spheroids vs. frequency.

spheroids, respectively, take the parameters ($\varepsilon_r = -1.4$, $\mu_r = -1.8$) and ($\varepsilon_r = -1.4 - j4.8, \mu_r = -1.8 - j2.5$). Orientation of random spheroids are assumed as non-uniform $\gamma \in [0°, 90°]$ and uniform $\beta \in [0°, 180°]$. Compared with the case of conventional dielectric spheroids [8], the backscattering σ_c, σ_x and m_s of metamaterial spheroids exhibit significantly asymmetry modes. In Figure 8 of the scattering pattern of lossless metamaterial spheroids, the maximum of σ_c shifts to the elliptic polarization ($\chi \neq 0$), the maximum of σ_x shifts in the opposite direction, and m_s of right-handed circular polarized wave ($\chi = -45°$) is the highest. These variations are related to non-uniform γ and constitutive parameters of metamaterial.

In Figure 9 of scattering pattern of lossy metamaterial spheroids, all maxims of σ_c, σ_x and m_s also demonstrate asymmetric shifts.

5 Conclusions

This paper derives the polarizability matrices and scattering amplitude functions of metamaterial spheroid. Based upon construction of the Mueller matrix solution, the bistatic scattering coefficients from a layer of random metamaterial spheroids are obtained. Co-polarized and cross-polarized bistatic and backscattering coefficients, polarization difference, polarizability degree, and their functional dependence upon metamaterial parameter are numerically simulated. The backscattering coefficients vary remarkably with frequency and take peaks at its resonance frequency. Asymmetric scattering pattern of a layer of random metamaterial spheroids are demonstrated and compared with dispersive FR-4 dielectric spheroids.

This work was supported by the China State Key Basis Research Project 2001CB309401 and China Natural Science Foundation No. 60171009.

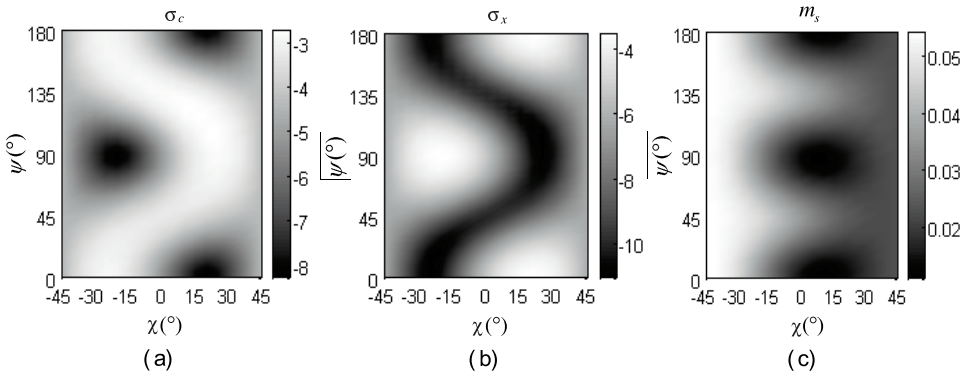

Fig. 8. σ_c, σ_x and m_s vs. (χ, ψ) of a layer of lossless metamaterial spheroids with non-uniform orientation distribution γ.

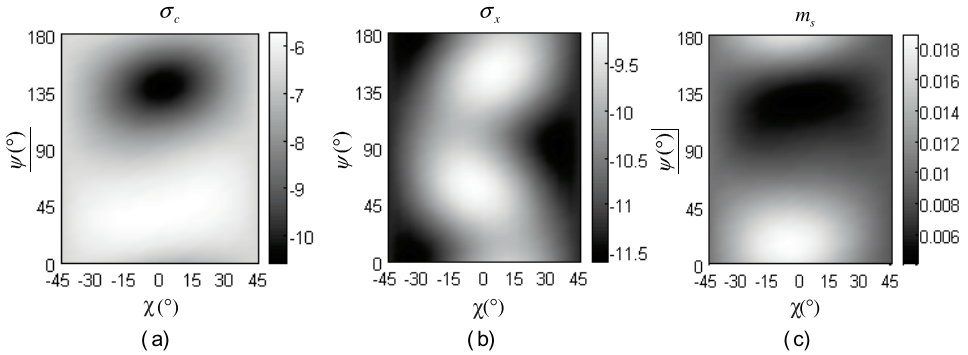

Fig. 9. σ_c, σ_x and m_s vs. (χ, ψ) of a layer of lossy metamaterial spheroids with non-uniform orientation distribution γ.

References

1. V.G. Veselago, Soviet Phys. USPEKI **10**, 509 (1968)
2. W. Rotman, IEEE T. Antenn. Propag. **10**, 82 (1962)
3. J.B. Pendry, F.J. Garcia Vidal, Computational studies of photonic band gaps in metals, *IEE Colloquium on Semiconductor Optical Microcavity Devices and Photonic Bandgaps* (Digest No. 1996/267) Dec. 1996: 5/1∼5/6
4. J.B. Pendry et al., IEEE T. Microw. Theory **47**, 2075 (1999)
5. D.R. Smith, W.J. Padilla, Phys. Rev. Lett. **84**, 4184 (2000)
6. J.B. Pendry, Phys. Rev. Lett. **85**, 3966 (2000)
7. N. Engheta, IEEE Antenn. Wireless Propag. Lett. **1**, 10 (2002)
8. Jin Y.Q. Jin, M. Chang, Electromagnetics **23**, 237 (2003)
9. Y.Q. Jin, Electromagnetic Scattering Modelling for Quantitative Remote Sensing (World Scientific, Singapore, 1993), pp. 32–64
10. L. Tsang, J.A. Kong, R. Shin, *Theory of Microwave Remote Sensing* (John Willey, New York, 1982)
11. Y.Q. Jin, J. Quant. Spectrosc. Ra. **48**, 295 (1992)
12. I.V. Lindell, A.H. Sihvola et al., *Electromagnetic Waves in Chiral and Bi-Isotropic Media* (Artech House Boston: London, 1994)
13. A. Ishimaru et al., IEEE T. Antenn. Propag. **51**, 2550 (2003)
14. H.Y. Yao, L.W. Li, Performance analysis of metamaterials with two-dimensional isotropy, *Proceedings of Annual Symposium of Singapore-MIT, 19-20 January 2004*, 58 (`https://dspace.mit.edu/handle/1721.1/3889`)
15. M.Y. Koledintseva, D.J. Pommerenke, J.L. Drewniak, FDTD analysis of printed circuit boards containing wideband Lorentzian dielectric dispersive meida, *IEEE International Symposium on Electromagnetic Compatibility, 19-23 Aug. 2002*, Vol. 2, pp. 830–833.